

# We are IntechOpen, the world's leading publisher of Open Access books Built by scientists, for scientists

5,800

Open access books available

142,000

International authors and editors

180M

Downloads

Our authors are among the

154

Countries delivered to

TOP 1%

most cited scientists

12.2%

Contributors from top 500 universities



WEB OF SCIENCE™

Selection of our books indexed in the Book Citation Index  
in Web of Science™ Core Collection (BKCI)

Interested in publishing with us?  
Contact [book.department@intechopen.com](mailto:book.department@intechopen.com)

Numbers displayed above are based on latest data collected.  
For more information visit [www.intechopen.com](http://www.intechopen.com)



# Topology Optimization Methods for Flexure Hinge Type Piezoelectric Actuators

*Shitong Yang, Yuelong Li, Guangda Qiao, Xiaosong Zhang and Xiaohui Lu*

## Abstract

Piezoelectric actuators have the obvious advantages of simple and compact structure, high precision and long stroke. However, it is difficult to satisfy the various industrial requirements. Topology optimization method can be used to find the new configurations of the compliant mechanism, and different objective function and constraint conditions can be flexibly used to determine the compliant mechanism. In the research of piezoelectric actuators, due to the advantages of compact structure, no lubrication and large displacement magnification, compliant mechanism is extremely suitable to be introduced into the design of piezoelectric actuators. In recent years, topology optimization method is frequently used to design the compliant mechanism on piezoelectric actuator, and has become a research hotspot. In this chapter, the development of topology optimization method is introduced, the design and research on the compliant mechanism of piezoelectric actuator have been summarized, and the future research direction and challenges of topology optimization design for flexure hinge type piezoelectric actuators are prospected.

**Keywords:** topology optimization, piezoelectric actuator, flexure hinge, compliant mechanism, displacement amplification

## 1. Introduction

Topology optimization method is firstly developed by Bendsøe and Kikuchi [1] and Bendsøe [2], which is originally used for an elastic material distribution problem in 1988. Compared with sizing and shape optimization, topology optimization is a more powerful tool, which allows new holes and connections to be generated in the design domain with a prescribed amount of material. Recently, the topology optimization method has been extended to many other fields, such as materials science [3, 4], micro-machines [5, 6], precision and ultra-precision machining [7, 8], optical focusing [9, 10], and so on. With the development of computer technology, topology

optimization is developing very fast, and the calculation process of topology optimization problem has been significantly simplified.

In the research of piezoelectric actuators, piezoelectric stacks are usually used in the driving field, which requires precise but minute motion [11, 12]. Flexure hinge type piezoelectric actuators are widely applied in precision machining, in-situ mechanical measurement, biomedicine and other fields because of its compact structure, long stroke and fast response speed [13–15]. The piezoelectric actuators are usually composed of piezoelectric stack, compliant mechanism and slider [16–20], here the compliant mechanisms are used as transmission and amplifying mechanisms. In the field of piezoelectric actuators, the modeling and design of compliant mechanisms are key issues. For example, bridge-type [21] and parallelogram-type [22] compliant mechanisms are applied to the reach of precision engineering. Sigmund [23, 24] has designed an inverting displacement amplifier, which has been used to obtain the maximum mechanical advantage. In addition, topology optimization methods have been assembled in commercial software [25], which makes the applications of topology optimization methods much easier.

There mainly three different types of topology optimization method are used to handle the design objectives and constraints of piezoelectric actuators: density-based methods, boundary variation methods, hard-kill methods, respectively [25, 26]. (1) Density-based methods, which include Solid Isotropic Material with Penalization (SIMP) and Rational Approximation of Materials Properties (RAMP) technique. (2) Boundary variation methods (level set and phase field). (3) Hard-kill methods, typically Evolutionary Structural Optimization (ESO) method and Bidirectional Evolutionary Structural Optimization (BESO) method. Many scholars have conducted in-depth research on the above three types of topology optimization method, the design theories and methods have developed rapidly. Topology optimization has becoming one of the important methods of piezoelectric actuator design.

However, topology optimization of piezoelectric actuators is a complicated problem, which contains the process of determining the connectivity, shape, and location of voids inside a given design domain. Traditional researches have given some topological structure for the design of piezoelectric actuators [27–34], the not solved problem is that which kind of compliant mechanisms with the flexure hinges makes the output performances best. Yang et al. [35] developed a static topology optimization method to solve the problem, and some topology optimization methods have also been extended to design the compliant mechanism of piezoelectric actuators [36–40]. At present, there is little research on using topology optimization method to design flexible hinges, and its theories and methods are very scarce, which has a lot of exploration space. Therefore, it is particularly important to explore the theories and methods of topology optimization for the design of flexure hinge type piezoelectric actuator.

We hope that this chapter will provide a summary of the recent advances and novel applications of topology optimization methods, provide exposure to lesser known, yet promising, techniques, and serve as a resource for those new to the field. The presentation of each method focuses on new developments and novel applications. So in Section 2, the operating principle of piezoelectric actuators is introduced, the problems are described and the topology optimization model is established, then the simulation analysis is performed. The prototype is fabricated and the experimental system is built in Section 3. Systematic experimental test is conducted to study the actual performance of the actuator in Section 4, and the conclusion and discussion of this chapter are in Section 5.

## 2. Operating principle and topology optimization method

### 2.1 Operation principle

The operating principle of the piezoelectric stick–slip actuator designed by the topology optimization method is shown in **Figure 1**. The asymmetric sawtooth wave is used as the excitation signal. A motion cycle can be divided into three phases:

**Initial phase** (as shown in **Figure 1a**): At time  $t_0$ , the input voltage is zero, so the piezoelectric stack is at its original length, the actuator is at rest, and the maximum static friction force between the indenter and slider is taken as the locking force  $F_0$ , point  $P$  is the contact point between the indenter and slider.

**Stick phase** (as shown in **Figure 1b**): From time  $t_0$  to  $t_1$ , the length of piezoelectric stack extends with the increases of voltage. Under the effect of flexure hinge, the driving mechanism produces oblique deformation. The vertical positive pressure  $Fy_1$

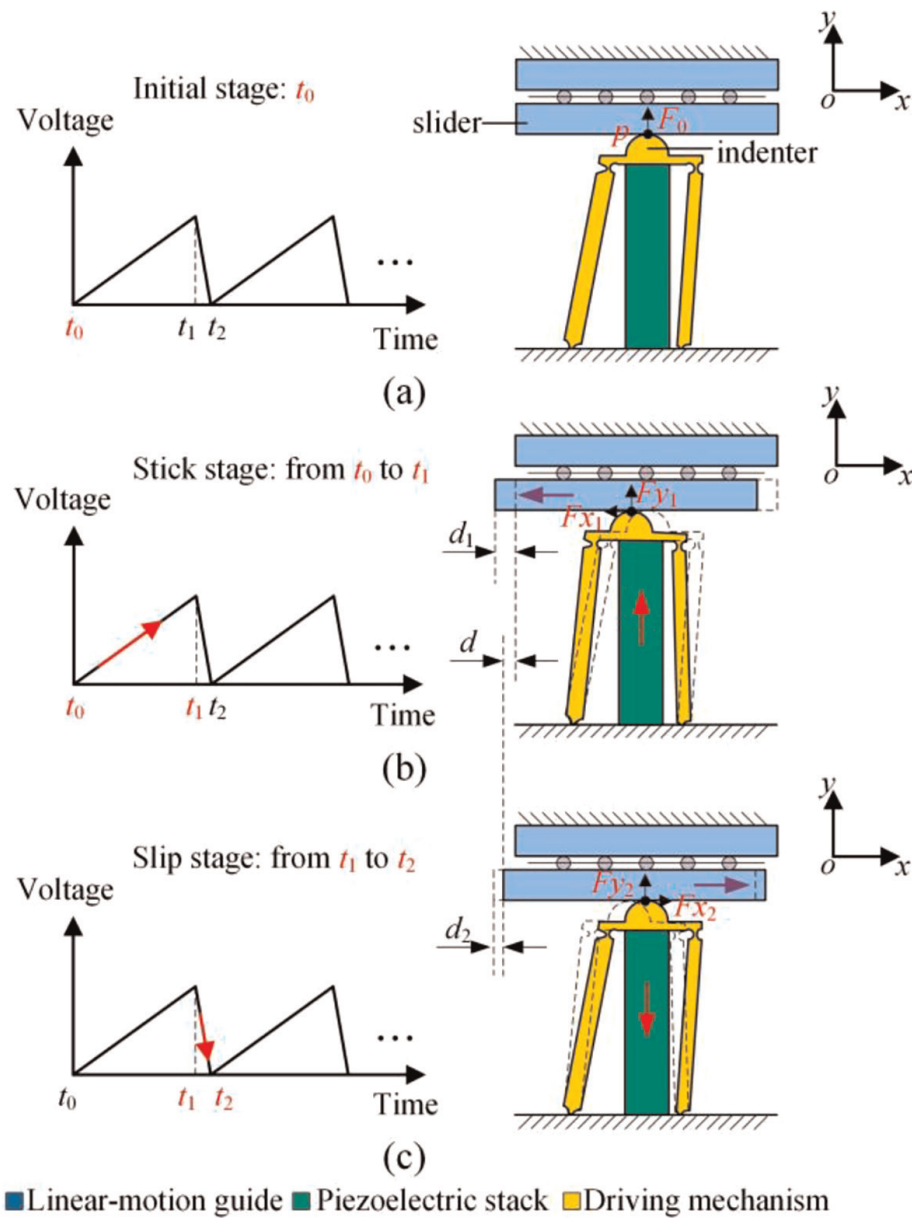


**Figure 1.** Operating principle: (a) initial phase. (b) Stick phase. (c) Slip phase.

on the slider increases, and the horizontal driving force  $Fx_1$  drives the slider to move  $d_1$  distance by static friction force, resulting in a large output displacement. When it reaches time  $t_1$ , the elongation of piezoelectric stack reaches the maximum.

**Slip phase** (as shown in **Figure 1c**): Contrary to the stick stage, the piezoelectric stack shrinks rapidly with the sudden drop of the input voltage, the driving mechanism returns to its original shape, and the vertical positive force  $Fy_2$  of the indenter against the slider decreases. There is relative sliding between the stator and the slider, resulting in horizontal kinetic friction force  $Fx_2$  in the opposite direction. When the action of kinetic friction force is greater than that of inertial force, a small backward displacement  $d_2$  occurs.

After one motion cycle, the slider moves a net forward distance  $d$ , and the actuator realizes a large-stroke output by repeating the above process driven by periodic asymmetric sawtooth wave.

## 2.2 Problem description

In order to better describe the method, the symbols used in the structural topology optimization process are expressed in **Table 1**.

Bendsøe and Sigmund pointed out that the ratio between output and input displacements is an important objective function for compliant mechanism [25]. The problem is how to find the optimal driving mechanism shape that can achieve the design goal in a certain design domain, and we design the driving mechanism on the basis of the theories of Ref. [25, 40].

Name	Symbol	Name	Symbol
Displacement vector	$\mathbf{u}$	Design domain volume	$V_0$
Input displacement	$u_{in}$	Prescribed volume fraction	$V_f$
Output displacement	$u_{out}^x$	Volume of element	$v_e$
Parasitic displacement	$u_{out}^y$	Total number of elements	$N$
Global stiffness matrix	$\mathbf{K}$	Penalization power	$p$
Element stiffness matrix	$\mathbf{k}_e$	Displacement magnification factor	$\lambda$
The element stiffness matrix for an element with unit Young's modulus	$\mathbf{k}_0$	Evaluation indicator	$\tau$
Global element stiffness matrix	$\mathbf{K}_e^0$	Minimum relative density value	$\rho_{\min}$
Input stiffness matrix	$\mathbf{K}_{in}$	Objective function	$g$
Output stiffness matrix	$\mathbf{K}_{out}$	Constraint function	$g_\tau, g_v$
Input stiffness	$k_{in}$	Adjoint unit load vector	$\mathbf{L}_x, \mathbf{L}_y, \mathbf{L}_{in}$
Output stiffness	$k_{out}$	Adjoint displacement vector	$\bar{\mathbf{u}}_x, \bar{\mathbf{u}}_y, \bar{\mathbf{u}}_{in}$
Input force vector	$\mathbf{f}_{in}$	Element of adjoint displacement vector	$(\bar{\mathbf{u}}_x)_e, (\bar{\mathbf{u}}_y)_e, (\bar{\mathbf{u}}_{in})_e$
Input force	$f_{in}$	Element of displacement vector	$\mathbf{u}_e$

**Table 1.**  
*The symbols of topology optimization method.*

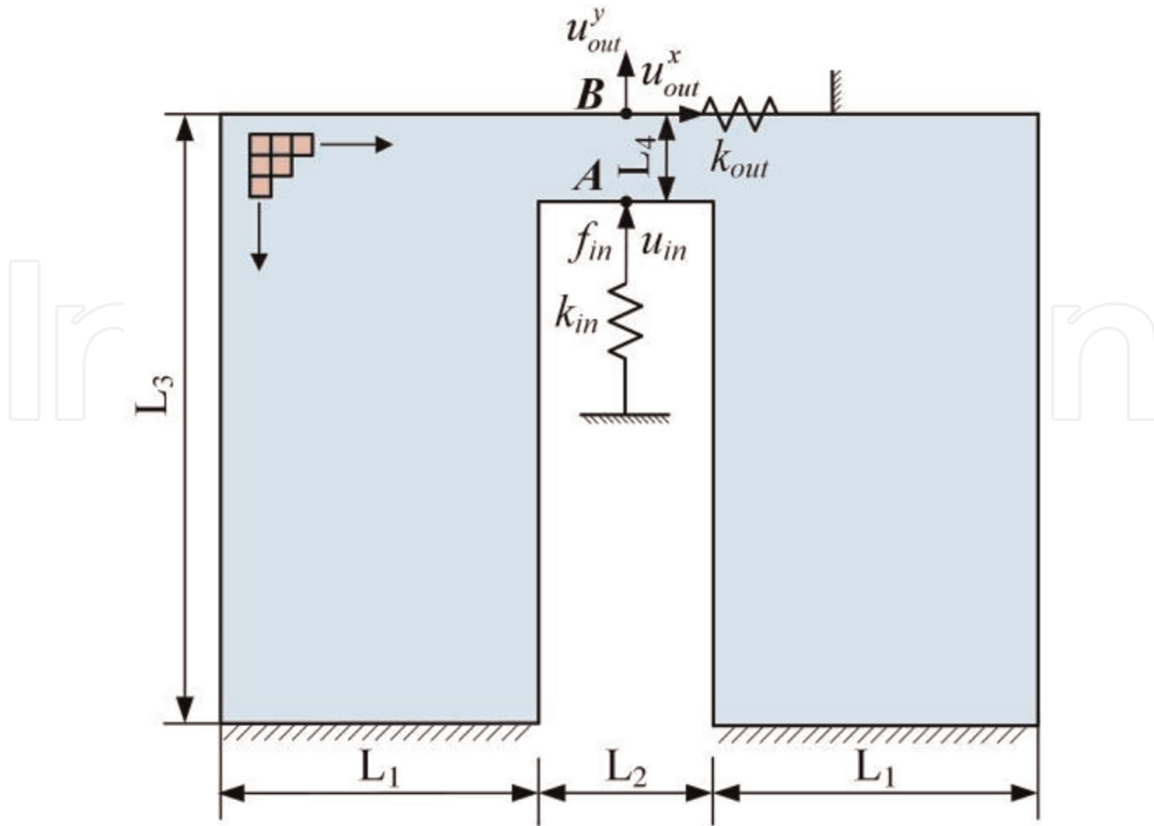


**Figure 2.**  
 The design domain of driving mechanism.

The structural characteristics of the stick–slip actuator are considered, the design domain of the flexure hinge mechanism is revealed in **Figure 2**, and the dimensions of the design domain are  $L_1 = 12.5$  mm,  $L_2 = 7$  mm,  $L_3 = 24$  mm,  $L_4 = 3.5$  mm, respectively.  $u_{out}^x$ ,  $u_{out}^y$ , and  $u_{in}$  are the output displacement at point B in  $x$  direction,  $y$  direction and the input displacement at point A, respectively.  $f_{in}$  is the input force,  $k_{in}$  and  $k_{out}$  are the stiffness of input spring and output spring, respectively.

The magnification factor  $\lambda$  is defined as the objective function, which is considered the relationship of output displacement  $u_{out}^x$  and input displacement  $u_{in}$ , while the parasitic displacement  $u_{out}^y$  is small, here the evaluation indicator  $\tau$  is defined as a constraint condition to restrict the parasitic displacement  $u_{out}^y$ .

The displacement magnification factor  $\lambda$  and evaluation indicator  $\tau$  are given as follows:

$$\lambda = \frac{u_{out}^x}{u_{in}} \quad (1)$$

$$\tau = \frac{u_{out}^y}{u_{out}^x} \quad (2)$$

### 2.3 Mathematical formulation

A basic engineering goal of piezoelectric stick–slip actuators is to maximize the stroke amplification in structures and mechanisms, a serious of different objective functions can be formulated. The basic topology optimization model of piezoelectric actuator can be given as:

$$\begin{aligned}
& \text{find } \boldsymbol{\rho} = [\rho_1, \rho_2, \dots, \rho_N]^T \in R^n \\
& \min g(\boldsymbol{\rho}) \\
& \text{s.t. } \left\{ g_j(\boldsymbol{\rho}) \leq 0, j = 1, 2, \dots, m \right\} \\
& g_v(\boldsymbol{\rho}) = \int_{\Omega} \rho dV \leq V_f V_0 \\
& \rho_i = 0 \text{ or } 1, i = 1, 2, \dots, n.
\end{aligned} \tag{3}$$

where  $\boldsymbol{\rho}$  is the vector of design variables,  $g(\boldsymbol{\rho})$  is the objective function,  $g_j(\boldsymbol{\rho})$  is the constraint functions,  $g_v(\boldsymbol{\rho})$  is the volume constraint function respectively.

The optimization models described in Eq. (3) are implemented using the MATLAB programming language. Usually, the design aim of the piezoelectric actuators is to maximize mechanical advantage, so the objective functions can be chosen as magnification factor and mechanical efficiency [23, 24], which can be used for static response. Although the compliant hinge is only a part of the compliant mechanism, and its motion and configuration are relatively simple, we can regard the compliant hinge as a simple compliant mechanism, so the topology optimization idea of the compliant mechanism is also applicable to the design of the compliant hinge. Sigmund [23, 24] developed an inverting displacement amplifier, and in [25] mechanical efficiency (ME) is defined as an objective function.

The objective function of the piezoelectric stick–slip actuator topology optimization problem is to obtain largest magnification factor  $\lambda$ , and the evaluation indicator  $\tau$  is used to restrict the parasitic displacement  $u_{out}^y$ . So the topology optimization model is given as follows:

$$\begin{aligned}
& \text{find } \boldsymbol{\rho} = [\rho_1, \rho_2, \dots, \rho_N]^T \in R^N \\
& \min g(\boldsymbol{\rho}) = -\frac{u_{out}^x}{u_{in}} \\
& \text{s.t. } \mathbf{K}\mathbf{u} = \mathbf{f}_{in} \\
& g_{\tau}(\boldsymbol{\rho}) = \left( \frac{u_{out}^y}{u_{out}^x} \right)^2 \leq \tau^* \\
& g_v(\boldsymbol{\rho}) = \sum_{e=1}^N v_e \rho_e \leq V_f V_0 \\
& 0 < V_f < 1 \\
& 0 < \rho_{\min} \leq \rho_e \leq 1, e = 1, 2, \dots, N.
\end{aligned} \tag{4}$$

where  $\mathbf{K}$  is the global stiffness matrix,  $\mathbf{u}$  is the global displacement vector and  $\mathbf{f}_{in}$  is input force vector, respectively.  $\boldsymbol{\rho}$  is the design variables vector,  $\rho_{\min}$  (usually  $\rho_{\min} = 0.001$ ) is introduced to avoid singularity case.  $v_e$  is the volume of element  $e$ ,  $V_0$  and  $V_f$  are the design domain volume and the prescribed volume fraction,  $N$  is the number of elements used to discretize the design domain, respectively.

The element stiffness matrix  $\mathbf{k}_e$  can be written as

$$\mathbf{k}_e = \rho_e^p \mathbf{k}_0 \tag{5}$$

where  $p$  represents the penalization power (typically  $p = 3$ ), and  $\mathbf{k}_0$  indicates the element stiffness matrix for an element with unit Young's modulus.

The global stiffness matrix  $\mathbf{K}$  can be expressed as

$$\mathbf{K} = \sum_{e=1}^N \rho_e^p \mathbf{K}_e^0 + \mathbf{K}_{in} + \mathbf{K}_{out} \quad (6)$$

where  $\mathbf{K}_e^0$  is the element stiffness matrix for an element with unit Young's modulus in global sense,  $\mathbf{K}_{in}$  is the stiffness matrix of the input spring  $k_{in}$  at the global level,  $\mathbf{K}_{out}$  is the stiffness matrix of the output spring  $k_{out}$  at the global level, respectively.

## 2.4 Sensitivity analysis

In this part, how to determinate the output displacement  $u_{out}^x$ , parasitic displacement  $u_{out}^y$  and input displacement  $u_{in}$  and their derivatives of  $\frac{\partial u_{out}^x}{\partial \rho_e}$ ,  $\frac{\partial u_{out}^y}{\partial \rho_e}$  and  $\frac{\partial u_{in}}{\partial \rho_e}$ , is a key problem. In addition, the relationships of  $u_{out}^x$ ,  $u_{out}^y$  and  $u_{in}$  can be considered as.

$$u_{out}^x = \mathbf{L}_x^T \mathbf{u}, \quad u_{out}^y = \mathbf{L}_y^T \mathbf{u}, \quad u_{in} = \mathbf{L}_{in}^T \mathbf{u} \quad (7)$$

where  $\mathbf{L}_x$ ,  $\mathbf{L}_y$  and  $\mathbf{L}_{in}$  are the vectors for which the inner product with  $\mathbf{u}$  produces the relevant output displacement  $u_{out}^x$ ,  $u_{out}^y$  and the relevant input displacement  $u_{in}$  ( $\mathbf{L}_x$ ,  $\mathbf{L}_y$  and  $\mathbf{L}_{in}$  are interpreted as a (unit) load vector), respectively.

The derivatives of  $u_{out}^x$ ,  $u_{out}^y$  and  $u_{in}$  can be expressed as

$$\frac{\partial u_{out}^x}{\partial \rho_e} = \mathbf{L}_x^T \frac{\partial \mathbf{u}}{\partial \rho_e} \quad (8)$$

$$\frac{\partial u_{out}^y}{\partial \rho_e} = \mathbf{L}_y^T \frac{\partial \mathbf{u}}{\partial \rho_e} \quad (9)$$

$$\frac{\partial u_{in}}{\partial \rho_e} = \mathbf{L}_{in}^T \frac{\partial \mathbf{u}}{\partial \rho_e} \quad (10)$$

Differentiating the static equation  $\mathbf{K}\mathbf{u} = \mathbf{f}_{in}$ , we have

$$\frac{\partial \mathbf{u}}{\partial \rho_e} = \mathbf{K}^{-1} \left( \frac{\partial \mathbf{f}_{in}}{\partial \rho_e} - \frac{\partial \mathbf{K}}{\partial \rho_e} \mathbf{u} \right) \quad (11)$$

Due to  $\mathbf{f}_{in}$  is a permanent load vector, we obtain

$$\frac{\partial \mathbf{f}_{in}}{\partial \rho_e} = 0 \quad (12)$$

Differentiating the global stiffness matrix, we have

$$\frac{\partial \mathbf{K}}{\partial \rho_e} = p \rho_e^{p-1} \mathbf{K}_e^0 = p \rho_e^{p-1} \mathbf{k}_0 \quad (13)$$

Next, we need to solve the adjoint equilibrium equations.

$$\mathbf{K}\bar{\mathbf{u}}_x = \mathbf{L}_x, \quad \mathbf{K}\bar{\mathbf{u}}_y = \mathbf{L}_y, \quad \mathbf{K}\bar{\mathbf{u}}_{in} = \mathbf{L}_{in} \quad (14)$$

where  $\bar{\mathbf{u}}_x$ ,  $\bar{\mathbf{u}}_y$  and  $\bar{\mathbf{u}}_{in}$  are the adjoint displacement vectors, which are determined by adjoint (unit) load vector  $\mathbf{L}_x$ ,  $\mathbf{L}_y$  and  $\mathbf{L}_{in}$ , respectively.

Combined with Eq. (8), Eqs. (11)–(14),  $\frac{\partial u_{out}^x}{\partial \rho_e}$  can be written as

$$\begin{aligned} \frac{\partial u_{out}^x}{\partial \rho_e} &= \mathbf{L}_x^T \frac{\partial \mathbf{u}}{\partial \rho_e} = \mathbf{L}_x^T \mathbf{K}^{-1} \left( \frac{\partial \mathbf{f}_{in}}{\partial \rho_e} - \frac{\partial \mathbf{K}}{\partial \rho_e} \mathbf{u} \right) \\ &= (\mathbf{K}^{-1} \mathbf{L}_x)^T \left( \frac{\partial \mathbf{f}_{in}}{\partial \rho_e} - \frac{\partial \mathbf{K}}{\partial \rho_e} \mathbf{u} \right) = -\bar{\mathbf{u}}_x^T \frac{\partial \mathbf{K}}{\partial \rho_e} \mathbf{u} \\ &= -p \rho_e^{p-1} \bar{\mathbf{u}}_x^T \mathbf{K}_e^0 \mathbf{u} = -p \rho_e^{p-1} (\bar{\mathbf{u}}_x)_e^T \mathbf{k}_0 \mathbf{u}_e \end{aligned} \quad (15)$$

Then we have

$$\frac{\partial u_{out}^y}{\partial \rho_e} = -p \rho_e^{p-1} (\bar{\mathbf{u}}_y)_e^T \mathbf{k}_0 \mathbf{u}_e \quad (16)$$

$$\begin{aligned} \frac{\partial u_{in}}{\partial \rho_e} &= -p \rho_e^{p-1} (\bar{\mathbf{u}}_{in})_e^T \mathbf{k}_0 \mathbf{u}_e \\ &= -p \rho_e^{p-1} \frac{\mathbf{u}_e^T \mathbf{k}_0 \mathbf{u}_e}{\|\mathbf{f}_{in}\|} \end{aligned} \quad (17)$$

where  $(\bar{\mathbf{u}}_x)_e$ ,  $(\bar{\mathbf{u}}_y)_e$ ,  $(\bar{\mathbf{u}}_{in})_e$  and  $\mathbf{u}_e$  are the elements of displacement vectors of  $\bar{\mathbf{u}}_x$ ,  $\bar{\mathbf{u}}_y$ ,  $\bar{\mathbf{u}}_{in}$  and  $\mathbf{u}$ , respectively.

The sensitivity of objective function  $g$  is found as

$$\frac{\partial g}{\partial \rho_e} = -\frac{\frac{\partial u_{out}^x}{\partial \rho_e} u_{in} - \frac{\partial u_{in}}{\partial \rho_e} u_{out}^x}{u_{in}^2} \quad (18)$$

and the sensitivity of constraint functions  $g_\tau$  and  $g_v$  can be expressed as

$$\frac{\partial g_\tau}{\partial \rho_e} = 2 \left( \frac{u_{out}^y}{u_{out}^x} \right) \frac{\frac{\partial u_{out}^y}{\partial \rho_e} u_{out}^x - \frac{\partial u_{out}^x}{\partial \rho_e} u_{out}^y}{u_{out}^x{}^2} \quad (19)$$

$$\frac{\partial g_v}{\partial \rho_e} = v_e \quad (20)$$

To avoid the checkerboards patterns and mesh dependencies phenomena, some restriction on the design must be imposed. Here a filtering technique is used to modify the sensitivity of  $\frac{\partial g}{\partial \rho_e}$  as follows:

$$\frac{\hat{\partial g}}{\partial \rho_e} = \frac{1}{\rho_e \sum_{k=1}^{N_k} H_k^e} \sum_{k=1}^{N_k} H_k^e \rho_k \frac{\partial g}{\partial \rho_k} \quad (21)$$

where  $N_k$  is the set of elements  $e$ ,  $dist(e, k)$  implies the center-to-center distance of element  $e$  and element  $k$ , which is smaller than the filter radius  $r_{min}$ , and the convolution operator (weight factor)  $H_k^e$  in Eq. (21) is defined as

$$H_k^e = \max (0, r_{\min} - dist(e, k)) \quad (22)$$

From Eq. (7) and Eqs. (15)–(17), the solutions of Eqs. (18), (19) are obtained.

**Figure 3** shows the flow chart of topology optimization procedures. Initially, the design domain, boundary conditions and material are defined, the design domain is discretized into finite element meshes and solve the static problem. Then the sensitivities of the objective function and constraint conditions are obtained, design variables are updated by MMA algorithm. Here the MMA algorithm is employed by Svanberg [41, 42] as the optimizer. Finally, check the convergence of the results, if it converges, the iteration will stop; if not, go to step 3.

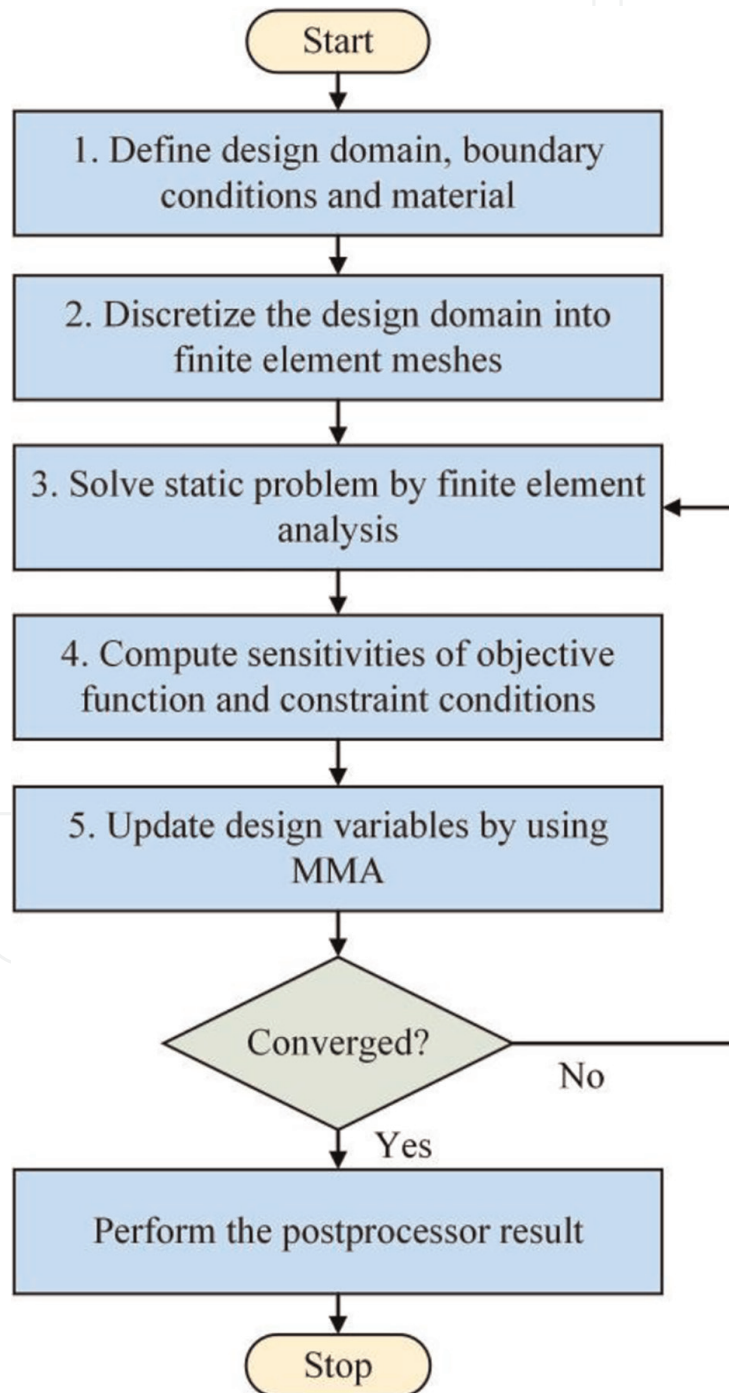


**Figure 3.**  
Flow chart of topology optimization procedures.

## 2.5 Numerical results and structural design

**Figure 2** shows that the design domain is divided into  $64 \times 48$  square four node elements, the side length of the element is 1, and the structural dimensions and material units are dimensionless. Based on the practical engineering experiments, the parameters in topology optimization model are chosen as follows: the volume fraction  $V_f$  is set to 0.2,  $\tau^*$  is set to  $10^{-4}$ , and the input stiffness  $k_{in}$  and output stiffness  $k_{out}$  in Eq. (6) are chosen as 10 and 0.001, respectively. and the input force is a unit force. For more details, we refer readers to Refs. [25,40].

**Figure 4** shows that the evaluation indicator  $\tau$  decrease significantly with the increase of iteration number. Therefore, the first constraint restriction in Eq. (4) markedly eliminates the effect of parasitic displacement  $u_{out}^y$  on the output displacement  $u_{out}^x$ . As shown in **Figure 5**, the displacement magnification factor  $\lambda$  raises with the increases of iteration number. With the continuous updating of design variables, the related topology optimization results are gradually converged.

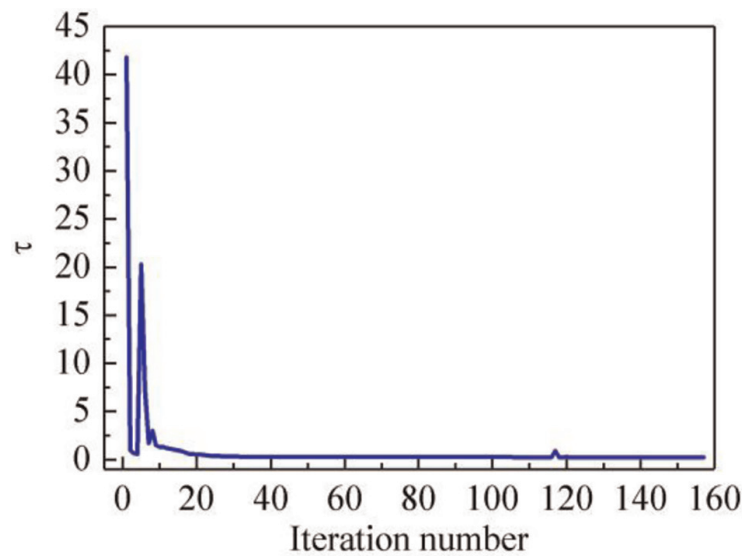


**Figure 4.**  
The relationship between the iteration number and evaluation indicator  $\tau$ .

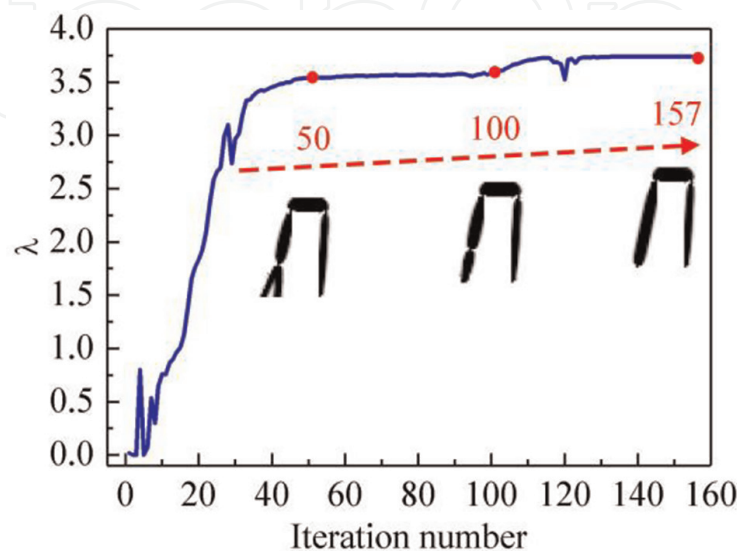


**Figure 5.**  
The relationship between the iteration number and displacement magnification factor  $\lambda$ .

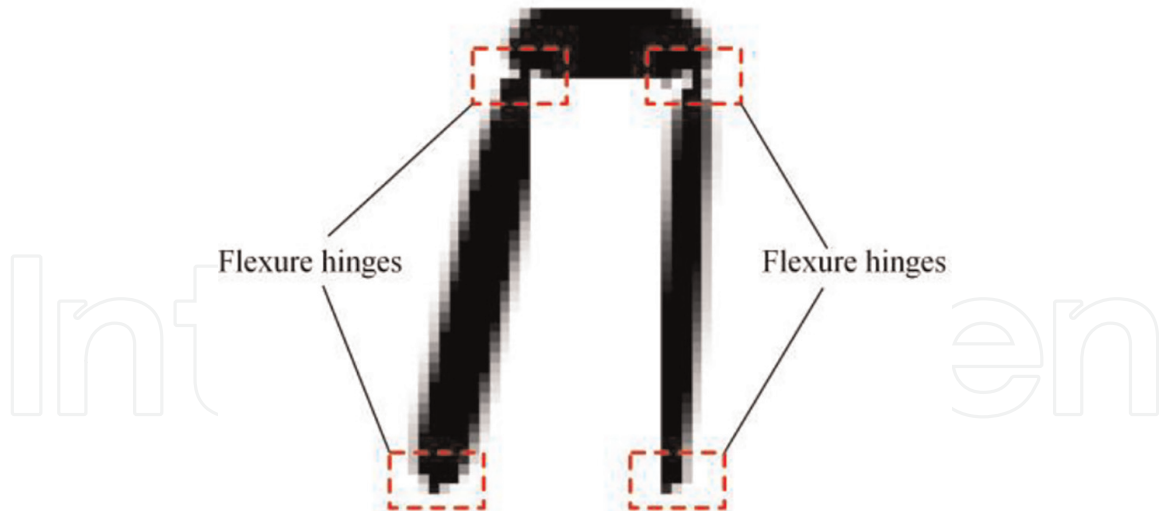


**Figure 6.**  
*The result of the topology optimization.*

**Figure 6** shows the topology optimization result, which is similar to the traditional four-bar mechanism, and the positions of the four flexure hinges and the tilt angles of the beams will be the main consideration in the mechanism design. Due to the gray unit in the topology image and the inaccurate contour extraction, the details of the hinges and boundaries of the structure are modified. **Figure 7** shows the main parameters of the driving mechanism, the overall dimension of the flexure hinge mechanism is  $32\text{ mm} \times 32\text{ mm} \times 9\text{ mm}$ , and an indenter with radius of  $2.5\text{ mm}$  is

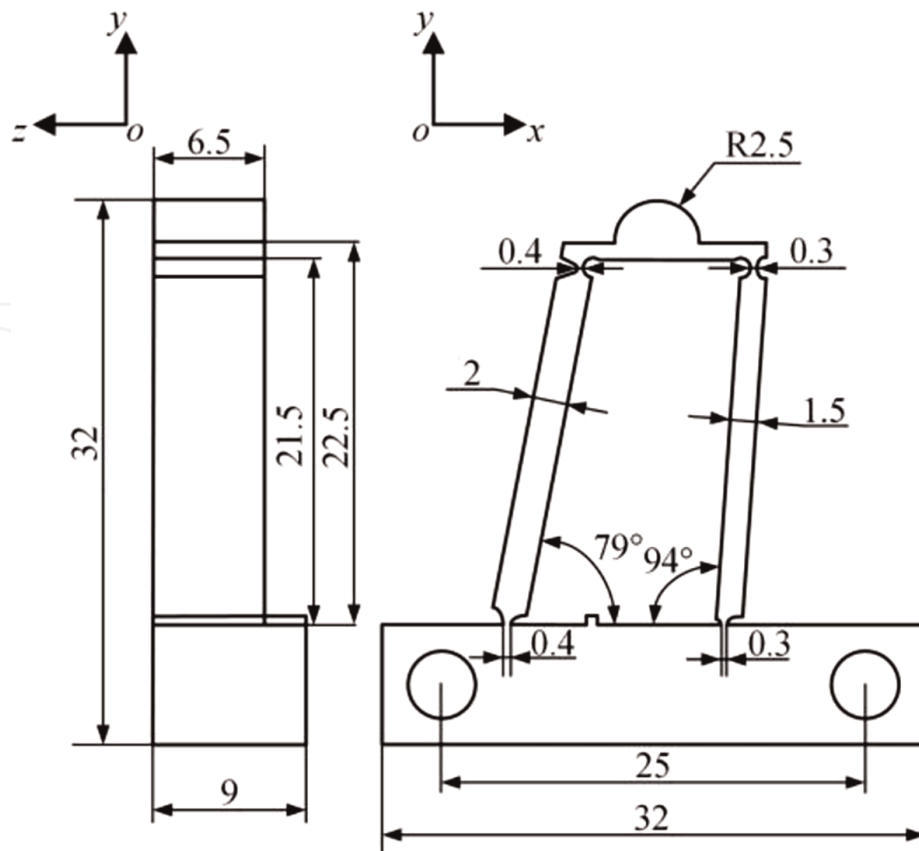


**Figure 7.**  
*Structural parameters of the driving mechanism. (unit: mm).*

selected to ensure that the driving mechanism can provide sufficient contact. The thicknesses of the four special-shaped flexure hinges are 0.3 mm, 0.3 mm, 0.4 mm and 0.4 mm, respectively.

## 2.6 Finite element analysis

Before the experimental verification, it is necessary to ensure that the flexure hinge driving mechanism can achieve the desired displacement amplification effect, thus the finite element analysis is carried out. AL7075 is selected as the material of the driving mechanism, the Young's modulus, density and Poisson's ratio of this material are  $7.17 \times 10^4$  MPa,  $2810 \text{ kg/m}^3$  and 0.33, respectively. Take the contact point  $P$  at the top of the driving mechanism as the reference, and the two holes are defined as fixed constraints. The elongation of the piezoelectric stack is set to  $10 \mu\text{m}$  to simulate the deformation of piezoelectric elements. The static simulation deformation is displayed in **Figure 8a**, the total displacement from point  $P$  to  $P'$  is  $52.415 \mu\text{m}$ , the displacement in the positive direction of  $y$ -axis direction is  $10.006 \mu\text{m}$ , and the displacement along the negative direction of the  $x$ -axis direction is  $51.195 \mu\text{m}$ . Then the analysis of equivalent stress is shown in **Figure 8b**, the maximum equivalent stress of the driving mechanism is 128.68 MPa near the point  $Q$ , which is less than the allowable stress of AL7075 to ensure the safe operation of the actuator. The static simulation results verify the feasibility and reliability of the flexure hinge driving mechanism. Further, the first-order mode of the mechanism is shown in **Figure 8c**. To ensure the operation stability of the actuator, the driving frequency should be lower than this value as much as possible.

## 3. Prototype configuration and experimental system construction

The prototype configuration of the developed actuator is shown in **Figure 9**. It mainly includes a slider, a stator, a preload mechanism and a base. The stator contains a piezoelectric stack, a driving mechanism, a preload screw and a shim block. The locking force is the maximum static friction force between the indenter and the slider, it can be adjusted by the preload mechanism. One end of the linear-motion guide is a slider for precise long-stroke motion, and the other end is fixed on the base. The base is used for fixing and supporting.

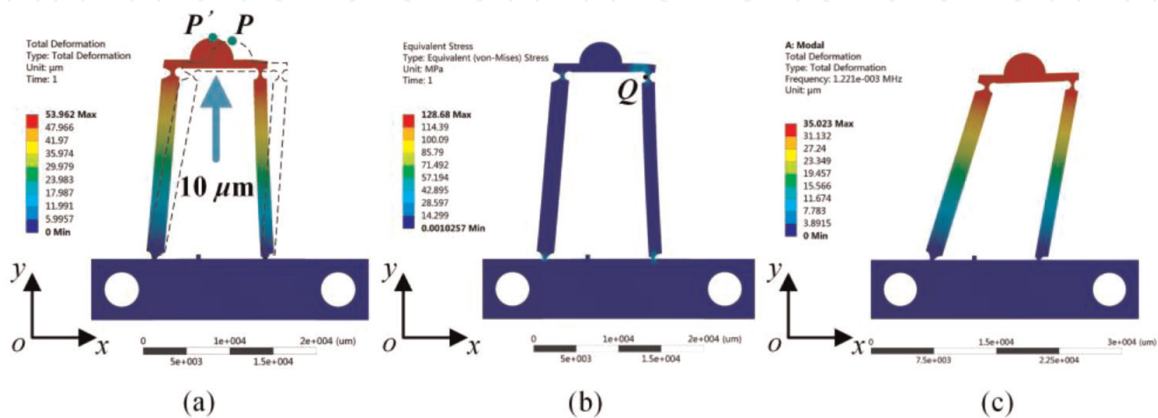


**Figure 8.** Simulation analysis by FEA: (a) the static simulation deformation. (b) Analysis of equivalent stress. (c) First-order mode of the mechanism.

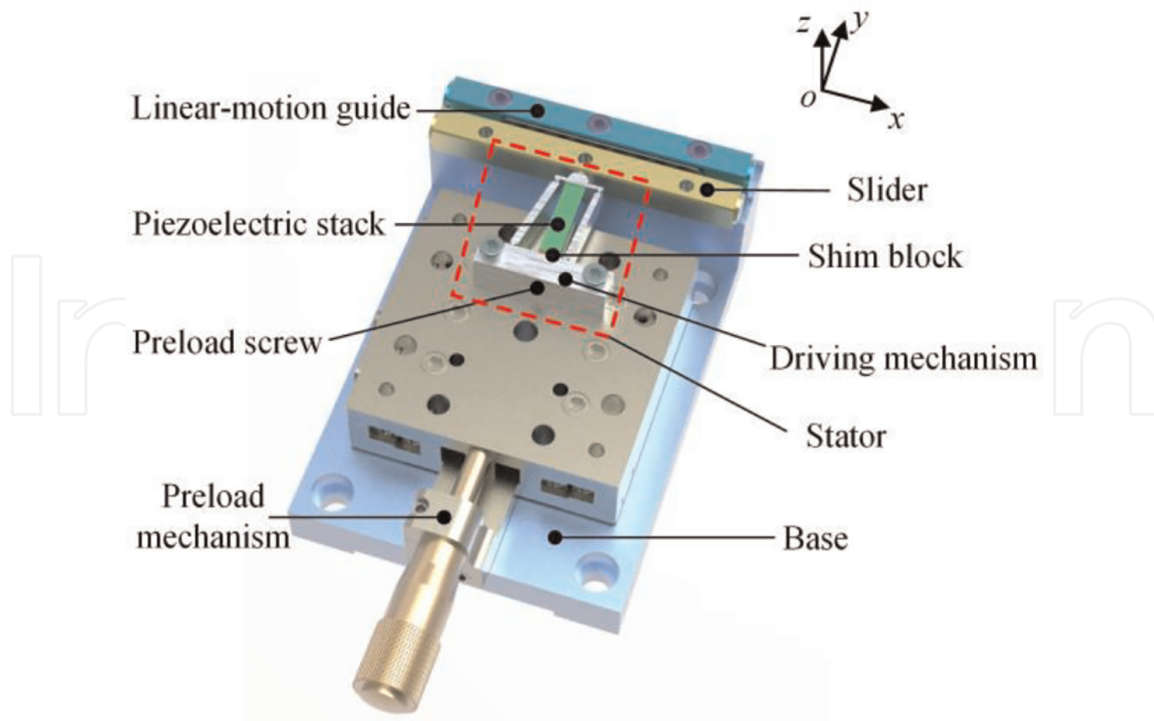


**Figure 9.**  
*Prototype configuration of the developed actuator.*

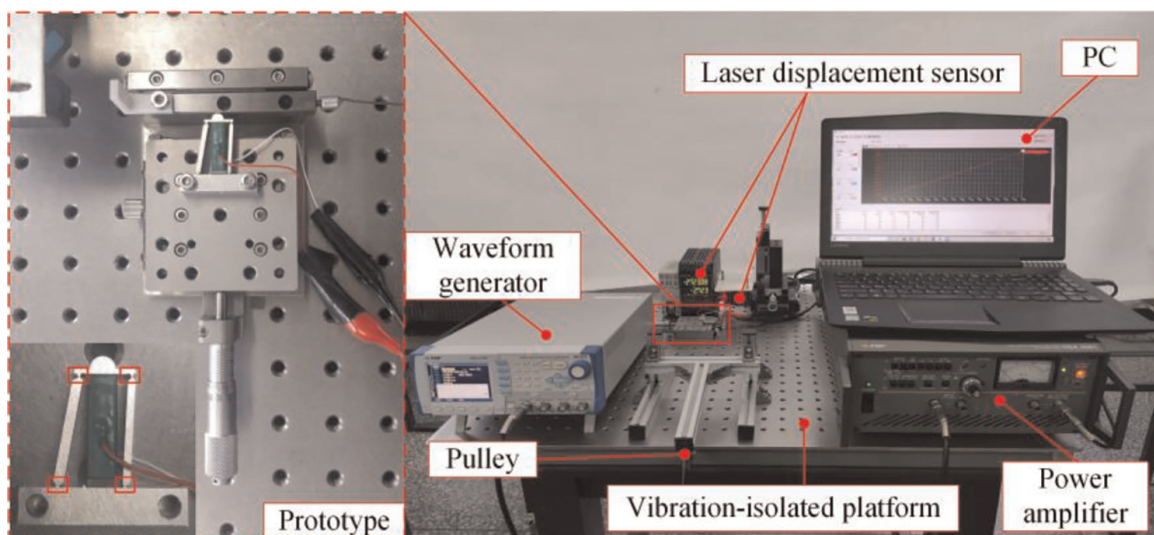


**Figure 10.**  
*The experimental system and the prototype.*

As shown in **Figure 10**, an experimental system is constructed to study the motion characteristics of the actuator. The experimental system mainly includes the prototype, a waveform generator, a power amplifier, a laser displacement sensor, a PC, a pulley, and a vibration-isolation platform. The asymmetric sawtooth wave is sent out by the waveform generator (WF 1974, Negative Feedback Corporation), then adjusted by the power amplifier (HSA 4051, Negative Feedback Corporation) as the excitation signal for the piezoelectric stack (AE0505D16). The motion characteristics are detected by the laser displacement sensor (LK-H020, Keyence Corporation), and saved in the PC. The pulley and wire are used to connect the slider and the weight, and the weight is used to calibrate the locking force and apply the load.

#### 4. Characteristic experiments

The driving voltage is set to  $100 V_{p-p}$ , and the frequency characteristics of the actuator under different locking forces are tested and shown in **Figure 11**. Under the locking force of 1 N, the maximum velocity is 15.25 mm/s at the frequency of 650 Hz; when the locking forces are 2 N and 3 N, the maximum velocities can be obtained at the frequency values of 700 Hz and 690 Hz, and the velocities are 12.48 mm/s and 9.67 mm/s, respectively.

Thus, there are corresponding different optimal frequencies under the different locking forces conditions. As displayed in **Figure 12**, the voltage characteristics under different locking forces are explored at the corresponding optimal frequency. It can be seen that the minimum starting voltage of the actuator increases with the increases of the locking force, and the minimum starting voltage of the actuator is  $21.5 V_{p-p}$  under the locking force of 1 N. In addition, the elongation of the piezoelectric stack increases as the voltage raises, the single step displacement of the actuator increases, thereby increasing the velocity. The motion resolution is also an important parameter of the actuator, which reflects the precise positioning characteristics of the actuator. It can

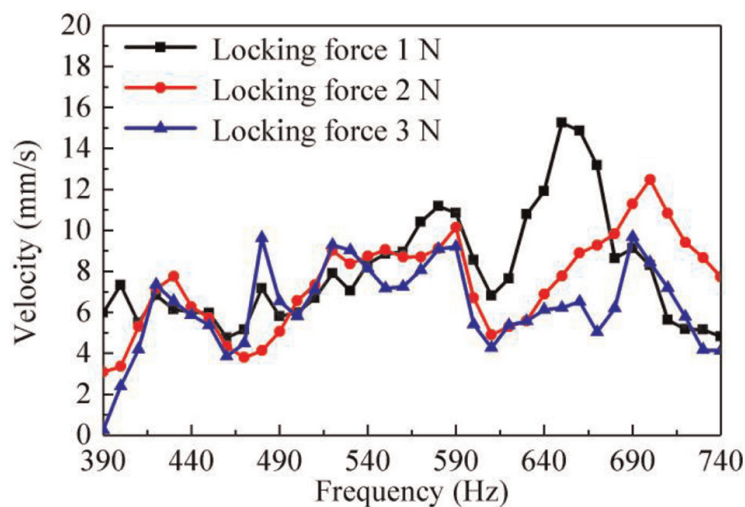


**Figure 11.**  
Frequency characteristics under different locking forces.

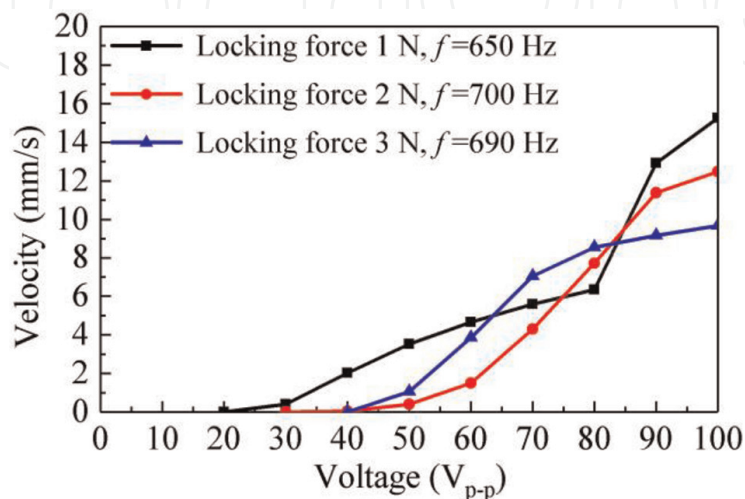


**Figure 12.**  
Voltage characteristics under different locking forces.

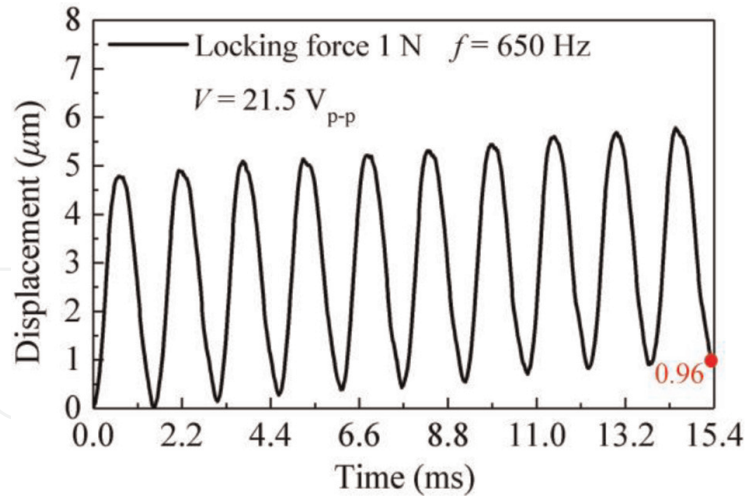


**Figure 13.**  
 The motion resolution under the locking force of 1 N.

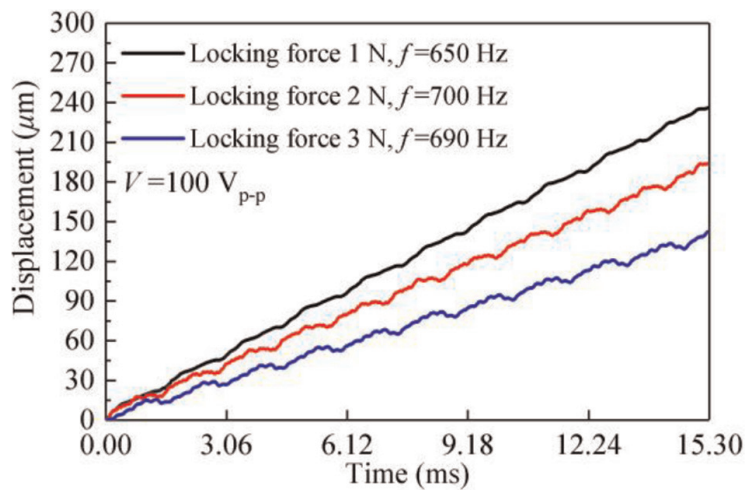


**Figure 14.**  
 Displacement characteristics under different locking forces.

be seen from **Figure 13**, the single step motion resolution of the actuator reaches 96 nm under the locking force of 1 N.

Maintaining the voltage is 100 V<sub>p-p</sub>, the displacement characteristics under different locking forces are plotted, as shown in **Figure 14**. It is obvious that the velocity is the fastest at the locking force of 1 N, the friction resistance is small at this time, so the backward motion is minimum. The load characteristics of the actuator is emerged in **Figure 15**, as the locking force gradually increases, the maximum load of the actuator increases significantly. Within a certain adjustment range, the greater locking force can increase the friction driving force, which improves the load capacity of the actuator. It can be seen that the velocity decreases almost linearly with the load increases, and the maximum load mass of the actuator exceeds 330 g under 3 N locking force.

The efficiency  $\eta$  is usually introduced to evaluate the output capacity of the actuator, which can be calculated by

$$\eta = \frac{P_{out}}{P_{in}} = \frac{F \times v}{P_{in}} = \frac{mg \times v}{P_{in}} \times 100\% \quad (23)$$

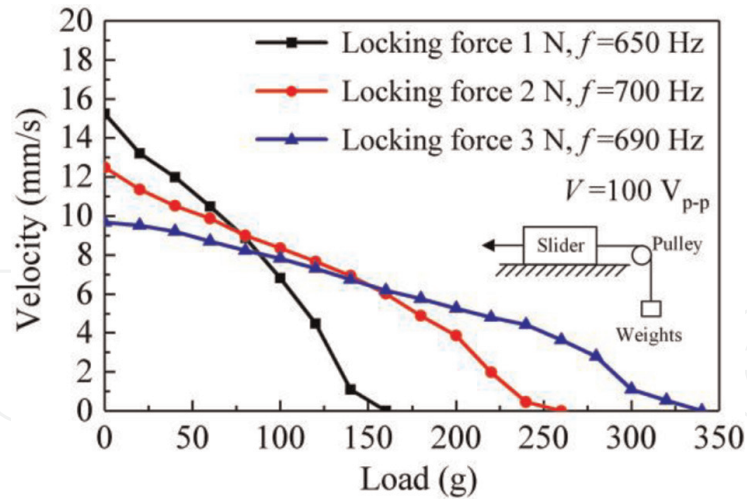


**Figure 15.**  
Load characteristics under different locking forces.

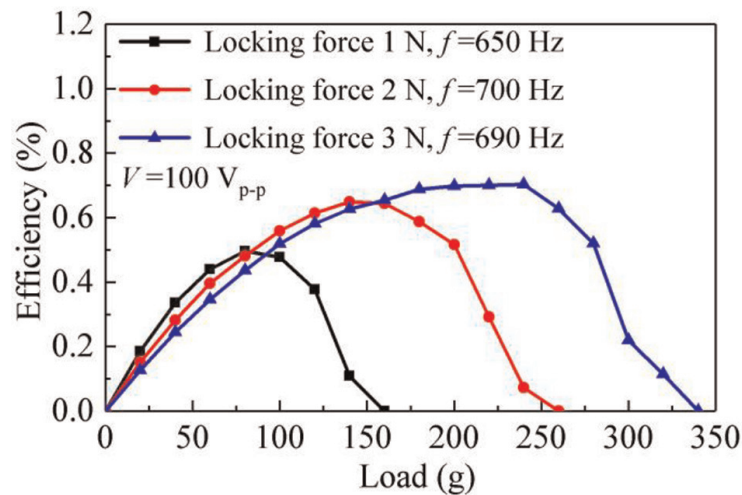


**Figure 16.**  
Efficiencies under different locking forces.

where  $P_{out}$  represents the output power,  $P_{in}$  represents the input power,  $F$  is the gravity load, and  $v$  is the output velocity, respectively. The input power can be detected by the power analyzer, and according to the load characteristics of actuator (in Figure 15), the output power  $P_{out}$  can be calculated.

Figure 16 shows that the efficiency of the actuator increases first and then decreases with the increases of load. It can be seen that when the locking force is 3 N, the efficiency of the actuator reaches the highest value 0.70% under the load of 240 g.

## 5. Conclusions

A topology optimization work of piezoelectric actuators is illustrated to improve their output performances. As shown in this chapter, topology optimization is a powerful tool for the design of piezoelectric actuators. The aim of this work is to serve as an introduction for those who are interested in the piezoelectric actuator optimization research field, and provide a reference work for scholars. It has to be pointed out that there remain a series of unsolved problems in the field of designing piezoelectric

actuators using topology optimization. In addition to the potential future work mentioned in each section, the following aspects should be considered to further promote the development of this research field: (1) The static topology optimization methods provide an efficient way to find the optimal design of piezoelectric actuators. However, some manufacturing-oriented static topology optimization methods for the design of piezoelectric actuators need to receive more attention. (2) Topology optimization of piezoelectric actuators considering dynamic problems is another important topic. When the loads changed rapidly, such as “stick–slip” type loads, the dynamic response problems of piezoelectric actuators should be concerned. (3) More topology optimization codes should be released, especially for the design of piezoelectric actuators. (4) Multi-materials topology optimization problem can be applied to piezoelectric actuators, the related theory should be considered by many outstanding scholars in the further.

## Acknowledgements

This work was financially supported by the Science and Technology Development Plan of Jilin Province (Nos. 20200201057JC and 20190201108JC), and the Technology Research Planning Project of Education Department of Jilin Province (No. JJKH20220690KJ).

The authors would like to thank K. Svanberg for providing the Matlab code of MMA optimizer.

## Conflict of interest

The author(s) declared no potential conflicts of interest with respect to the research, authorship, and/or publication of this article.

## Author details

Shitong Yang, Yuelong Li, Guangda Qiao, Xiaosong Zhang and Xiaohui Lu\*  
School of Mechatronic Engineering, Changchun University of Technology,  
Changchun, China

\*Address all correspondence to: [luxh13@ccut.edu.cn](mailto:luxh13@ccut.edu.cn)

## IntechOpen

© 2022 The Author(s). Licensee IntechOpen. This chapter is distributed under the terms of the Creative Commons Attribution License (<http://creativecommons.org/licenses/by/3.0>), which permits unrestricted use, distribution, and reproduction in any medium, provided the original work is properly cited. 

## References

- [1] Bendsøe MP, Kikuchi N. Generating optimal topologies in structural design using a homogenization method. *Computer Methods in Applied Mechanics and Engineering*. 1988;**71**: 197-224. DOI: 10.1016/0045-7825(88)90086-2
- [2] Bendsøe MP. Optimal shape design as a material distribution problem. *Structural optimization*. 1989;**1**:193-202. DOI: 10.1007/BF01650949
- [3] Bhowmick S, Hintsala E, Stauffer D, Syed Asif SA. In-situ SEM and TEM nanomechanical study of wear and failure mechanisms. *Microscopy and Microanalysis*. 2018;**24**:1934-1935. DOI: 10.1017/S1431927618010152
- [4] Breguet JM, Driesen W, Kaegi F, Cimprich T. Applications of Piezo-Actuated Micro-Robots in Micro-Biology and Material Science. Harbin, China: 2007 International Conference on Mechatronics and Automation; 5–8 August 2007, IEEE; 2007. pp. 57-62
- [5] Wang L, Chen W, Liu J, Deng J, Liu Y. A review of recent studies on non-resonant piezoelectric actuators. *Mechanical Systems and Signal Processing*. 2019;**133**:106254. DOI: 10.1016/j.ymssp.2019.106254
- [6] Wang S, Rong W, Wang L, Pei Z, Sun L. Design, analysis and experimental performance of a novel stick-slip type piezoelectric rotary actuator based on variable force couple driving. *Smart Materials and Structures*. 2017;**26**: 055005. DOI: 10.1088/1361-665X/aa64c3
- [7] Liu Y, Wang L, Gu Z, Quan Q, Deng J. Development of a two-dimensional linear piezoelectric stepping platform using longitudinal-bending hybrid actuators. *IEEE Transactions on Industrial Electronics*. 2019;**66**: 3030-3040
- [8] Tian Y, Zhang D, Shirinzadeh B. Dynamic modelling of a flexure-based mechanism for ultra-precision grinding operation. *Precision Engineering*. 2001; **35**:554-565
- [9] Cherepanov V, Coenen P, Voigtländer B. A nano-positioner for scanning probe microscopy: The KoalaDrive. *Review of Scientific Instruments*. 2012;**83**:023703. DOI: 10.1063/1.3681444
- [10] Kratochvil BE, Dong L, Nelson BJ. Real time rigid-body visual tracking in a scanning electron microscope. *The International Journal of Robotics Research*. 2009;**28**:498-511. DOI: 10.1177/0278364908099849
- [11] Cheng T, He M, Li H, Lu X, Zhao H, Gao H. A novel trapezoid-type stick-slip piezoelectric linear actuator using right circular flexure hinge mechanism. *IEEE Transactions on Industrial Electronics*. 2017;**64**:5545-5552. DOI: 10.1109/TIE.2017.2677318
- [12] Lu X, Gao Q, Li Y, Yu Y, Zhang X, Qiao G, et al. A linear piezoelectric stick-slip actuator via triangular displacement amplification mechanism. *IEEE Access*. 2020;**8**:6515-6522. DOI: 10.1109/ACCESS.2019.2963680
- [13] Oubellil R, Voda A, Boudaoud M, Régnier S. Mixed stepping/scanning mode control of stick-slip SEM-integrated nano-robotic systems. *Sensors and Actuators A: Physical*. 2019;**285**: 258-268. DOI: 10.1016/j.sna.2018.08.042
- [14] Gao X, Zhang S, Deng J, Liu Y. Development of a small two-dimensional

robotic spherical joint using a bonded-type piezoelectric actuator. *IEEE Transactions on Industrial Electronics*. 2021;**68**:724-733. DOI: 10.1109/TIE.2019.2959475

[15] Le T, Danh LT, Jeon JU. A proposal of a piezo rotary positioning device: Design, modeling and experiments. *Smart Materials and Structures*. 2019;**28**:115032. DOI: 10.1088/1361-665X/ab4736

[16] Canfield S, Frecker M. Topology optimization of compliant mechanical amplifiers for piezoelectric actuators. *Structural and Multidisciplinary Optimization*. 2000;**20**:269-279. DOI: 10.1007/s001580050157

[17] Claeysen F, Letty RL, Barillot F, Sosnicki O. Amplified piezoelectric actuators: Static and dynamic applications. *Ferroelectrics*. 2007;**351**:3-14. DOI: 10.1080/00150190701351865

[18] Guo Z, Tian Y, Zhang D, Wang T, Wu M. A novel stick-slip based linear actuator using bi-directional motion of micropositioner. *Mechanical Systems and Signal Processing*. 2019;**128**:37-49. DOI: 10.1016/j.ymssp.2019.03.025

[19] Huang H, Zhao H, Fan Z, Zhang H, Ma Z, Yang Z. Analysis and experiments of a novel and compact 3-DOF precision positioning platform. *Journal of Mechanical Science and Technology*. 2013;**27**:3347-3356. DOI: 10.1007/s12206-013-0856-6

[20] Hunstig M, Hemsell T, Sextro W. Stick-slip and slip-slip operation of piezoelectric inertia drives. Part I: Ideal excitation. *Sensors and Actuators A: Physical*. 2013;**200**:90-100. DOI: 10.1016/j.sna.2012.11.012

[21] Li J, Zhou X, Zhao H, Shao M, Hou P, Xu X. Design and experimental performances of a piezoelectric linear

actuator by means of lateral motion. *Smart Materials and Structures*. 2015;**24**:065007. DOI: 10.1088/0964-1726/24/6/065007

[22] Li J, Zhou X, Zhao H, Shao M, Li N, Zhang S, et al. Development of a novel parasitic-type piezoelectric actuator. *IEEE/ASME Transactions on Mechatronics*. 2017;**22**:541-550. DOI: 10.1109/TMECH.2016.2604242

[23] Sigmund O. On the design of compliant mechanisms using topology optimization. *Mechanics of Structures and Machines*. 1997;**25**:493-524. DOI: 10.1080/08905459708945415

[24] Sigmund O. A 99 line topology optimization code written in Matlab. *Structural and Multidisciplinary Optimization*. 2001;**21**:120-127. DOI: 10.1007/s001580050176

[25] Bendsoe MP, Sigmund O. *Topology Optimization: Theory: Methods and Applications*. Berlin: Springer; 2004

[26] Da D. *Topology Optimization Design of Heterogeneous Materials and Structures*. Hoboken: Wiley; 2019

[27] Li Y, Li H, Cheng T, Lu X, Zhao H, Chen P. Note: Lever-type bidirectional stick-slip piezoelectric actuator with flexible hinge. *Review of Scientific Instruments*. 2018;**89**:086101. DOI: 10.1063/1.5038640

[28] Li J, Huang H, Morita T. Stepping piezoelectric actuators with large working stroke for nano-positioning systems: A review. *Sensors and Actuators A: Physical*. 2019;**292**:39-51. DOI: 10.1016/j.sna.2019.04.006

[29] Hunstig M. Piezoelectric inertia motors: A critical review of history, concepts, design, applications, and

perspectives. *Actuators*. 2017;**6**:7.  
DOI: 10.3390/act6010007

[30] Iqbal S, Malik A. A review on MEMS based micro displacement amplification mechanisms. *Sensors and Actuators A: Physical*. 2019;**300**:111666.  
DOI: 10.1016/j.sna.2019.111666

[31] Kang D, Lee MG, Gweon D. Development of compact high precision linear piezoelectric stepping positioner with nanometer accuracy and large travel range. *Review of Scientific Instruments*. 2007;**78**:075112.  
DOI: 10.1063/1.2756627

[32] Kim JH, Kim SH, Kwak YK. Development of a piezoelectric actuator using a three-dimensional bridge-type hinge mechanism. *Review of Scientific Instruments*. 2003;**74**:2918.  
DOI: 10.1063/1.1569411

[33] Lau GK, Du HJ, Guo NQ, Lim MK. Systematic design of displacement-amplifying mechanisms for piezoelectric stacked actuators using topology optimization. *Journal of Intelligent Material Systems and Structures*. 2000;**11**:685-695. DOI: 10.1106/17V9-DR0Q-6BMU-RKUY

[34] Lee HJ, Kim HC, Kim HY, Gweon DG. Optimal design and experiment of a three-axis out-of-plane nano positioning stage using a new compact bridge-type displacement amplifier. *Review of Scientific Instruments*. 2013;**84**:115103.  
DOI: 10.1063/1.4827087

[35] Yang S, Li Y, Xia X, Ning P, Ruan W, Zheng R, et al. A topology optimization method and experimental verification of piezoelectric stick-slip actuator with flexure hinge mechanism. *Archive of Applied Mechanics*. 2022;**92**: 271-285. DOI: 10.1007/s00419-021-02055-4

[36] Ling M, Cao J, Zeng M. Enhanced mathematical modeling of the displacement amplification ratio for piezoelectric compliant mechanisms. *Smart Materials and Structures*. 2016;**25**: 075022. DOI: 10.1088/0964-1726/25/7/075022

[37] Liu K, Tovar A. An efficient 3D topology optimization code written in Matlab. *Structural and Multidisciplinary Optimization*. 2014;**50**:1175-1196.  
DOI: 10.1007/s00158-014-1107-x

[38] Schlinquer T, Mohand-Ousaid A, . Rakotondrabe M. Displacement Amplifier Mechanism for Piezoelectric Actuators Design Using SIMP Topology Optimization Approach. In: 2018 IEEE International Conference on Robotics and Automation (ICRA); 21–25 May 2018; Brisbane, QLD, Australia: IEEE; 2018. p. 4305–4311

[39] Yang S, Xia X, Liu X, Qiao G, Zhang X, Lu X. Improving velocity of stick-slip piezoelectric actuators with optimized flexure hinges based on SIMP method. *IEEE Access*. 2020;**8**: 213122-213129. DOI: 10.1109/ACCESS.2020.3039857

[40] Zhang X, Zhu B. *Topology Optimization of Compliant Mechanisms*. Singapore: Springer; 2018

[41] Svanberg K. The method of moving asymptotes—A new method for structural optimization. *International Journal for Numerical Methods in Engineering*. 1987;**24**: 359-373. DOI: 10.1002/nme.1620240207

[42] Svanberg K. MMA and GCMMA—Two Methods for Nonlinear Optimization [Internet]. 2007. Available from: <https://people.kth.se/~krille/mmagcmma.pdf>. [Accessed: May 2, 2022]